THE JOURNAL OF PHYSICAL CHEMISTRY C

Article

pubs.acs.org/JPCC

Pure Hexagonal Phase of EuF_3 Modulated by High Pressure

Qian Li,[†] Shourui Li,[†] Kai Wang,*[,†] Jing Liu,[‡] Bingbing Liu,[†] Ke Yang,[§] and Bo Zou*[,†]

[†]State Key Laboratory of Superhard Materials, Jilin University, Changchun 130012, China

[‡]Beijing Synchrotron Radiation Laboratory, Institute of High Energy Physics, Chinese Academy of Sciences, Beijing 100039, China

[§]Shanghai Synchrotron Radiation Facilities, Shanghai Institute of Applied Physics, Chinese Academy of Sciences, Shanghai 201204, China

ABSTRACT: We have performed in situ high-pressure synchrotron X-ray diffraction (XRD) and photoluminescence (PL) measurements to explore the behaviors of europium fluoride (EuF_3). At ambient conditions, EuF_3 consists of two representative phases of the rare earth trifluorides family. The orthorhombic phase (α-EuF_3) evolves into its hexagonal phase (β-EuF_3) in the pressure range 2.7−7.8 GPa, which involves the variations of europium positions in one layer and changes in the coordination number of europium from nine to eleven. The existence of pure β-EuF_3 at high pressure allows solving detailed structural information of β-EuF_3 for the first time. In comparison with the excellent hydrostatic condition in methanol−ethanol−water, a somewhat poor pressure condition in silicon oil contributes to the sluggishness of the phase transition, restrains the compression of lattice constants, and controls the phase content ratio of the quenched sample. Significantly, the PL measurements show that the pressure-induced purity of EuF_3 is a benefit to the enhancement of its luminescence intensity. This work provides precise structural and PL information on β-EuF_3, getting a deeper insight into the nature of these two typical structures with respect to rare-earth trifluorides.

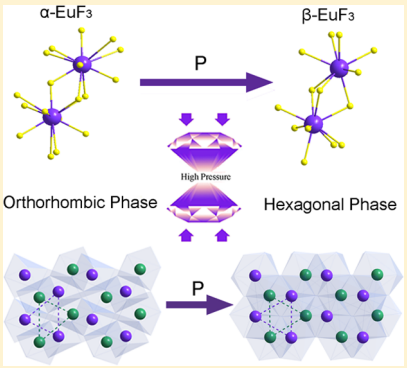

INTRODUCTION

Rare earth trifluorides (REF_3), a famous family of functional material, have received considerable attention for a long time.[1−5] Such intense interest stems from their unique luminescence properties and widespread technological applications in optical, optoelectronics, chemical, and biology fields.[6−10] Research has shown that the advanced materials' functions are strongly dependent on their morphologies and structures. Exploring the structural evolution in the REF_3 family provides a deeper insight into the structure−property relationship and new insights into the nature of REF_3 structures. Europium fluoride (EuF_3) crystallizes in two typical REF_3 structures at ambient conditions. As a basic member of REF_3 family, it can be chosen to explore the high pressure behaviors of typical REF_3 structures. It is expected that the transition path between the two typical REF_3 structures will be obtained through the study of EuF_3.[11,12] Meanwhile, the extensive applications of EuF_3 also promote the deeper investigation of its functional properties. Numerous synthetic chemical efforts have been devoted to control the sizes, morphologies, structures, and properties of EuF_3.[13−17] However, it is still an open question that whether and how physical methods tune its structure and properties.

Pressure, the most significant thermodynamic parameter, can reduce the interatomic distance, and thus vary the interactions and electronic structure in materials effectively. It is a powerful method to modulate the structures, generate new properties, and unravel the phenomena hidden at ambient conditions.[18,19] Since Eu^{3+} is extremely sensitive to structural changes in the environment (site symmetry, surface vs bulk Eu^{3+}),[20] introducing high pressure to EuF_3 is expected to obtain information on the relationship between two typical REF_3 structures, and the photoluminescence (PL) properties correspondingly.[21−23] Meanwhile, high-pressure studies on EuF_3 also show the stability of the material, which is essential for its practical viability, and expand the phase diagram of REF_3.[24,25]

At ambient conditions, the REF_3 family shows two main structures. One is the hexagonal tysonite structure type for low-Z rare earth elements, ranging from elements La to Nd. Another one is the orthorhombic β-YF_3 structure type for the remainder of the mid/high-Z rare earth elements, Sm to Lu.[26] Europium is the intermediate element in the Lanthanide series. It is noteworthy that EuF_3 can crystallize in two polymorphic modifications simultaneously at ambient conditions, the orthorhombic β-YF_3 phase of α-EuF_3 and hexagonal tysonite phase of β-EuF_3. In other words, EuF_3 is able to exist as mixed phases material at ambient conditions.[11,12] It is worth noting that β-EuF_3 is the high-temperature phase of EuF_3.[11] During industrial manufacture and ordinary synthesis processes, heating dehydration of EuF_3 is commonly used, so that EuF_3 is always obtained as the mixed phases. Therefore, deeper exploration on the mixed phases of EuF_3 becomes necessary and possesses more practical significance.

The structure of α-EuF_3 has been well characterized (Figure 1) and belongs to orthorhombic space group *Pnma* with $Z = 4$ in one unit cell, the unit cell parameters being $a = 6.6105$ Å, $b = 7.0157$ Å, $c = 4.3959$ Å.[27] This structure consists of the

Received: December 17, 2013
Revised: February 24, 2014
Published: March 18, 2014

   dx.doi.org/10.1021/jp412366y | J. Phys. Chem. C 2014, 118, 7562−7568

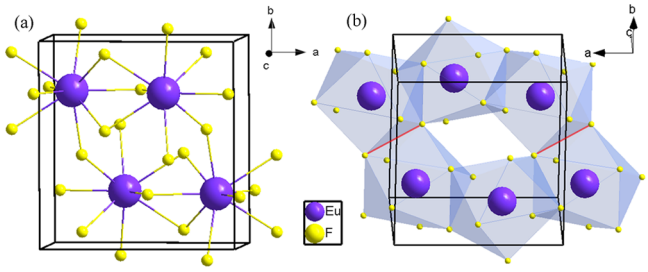

Figure 1. The crystal structure of α-EuF_3 at ambient conditions. (a) one unit cell; (b) overlapped six-tricapped-prism cycles. Two red lines represent the edges connecting two prisms to form pairs.

overlapped six-tricapped-prism cycles, in which four junctions are faces and the other two are edges (marked by red lines). β-EuF_3 crystallizes in trigonal space group $P\bar{3}c1$ (a = 6.9204 Å, c = 7.0856 Å, JCPDS No. 32-0373) with Z = 6 in one unit cell. However, more detailed structural information of β-EuF_3, including atomic positions and arrangement, has not been solved so far. Meanwhile, the relationship and transition path between the ambient and high-pressure phases of EuF_3 remain to be explored.

Hence, introducing high pressure to the mixed phases EuF_3 is expected to obtain not only further structural information on β-EuF_3, but also a deeper insight into the transition path and mechanism between the two typical ambient structures of REF_3. This is of crucial importance for REF_3 in understanding their structural evolution and structure−property relationships. Meanwhile, considering the functionality of EuF_3, extreme conditions can be encountered during the application. Therefore, a thorough high-pressure study on its structure and PL property may helpful for the further application of EuF_3.

Angle-dispersive synchrotron X-ray diffraction (ADXRD), combined with the diamond anvil cell (DAC) technique, is a powerful tool to monitor the structural evolution at high pressure, and PL measurement offers information on the emission lines of Eu^{3+}, as the probe of the chemical environment and structural variation. Therefore, in this work, we have performed in situ high-pressure ADXRD and PL measurements to explore the behaviors of europium fluoride (EuF_3) up to the pressure of ~10 GPa.

EXPERIMENTAL SECTION

Powdered EuF_3 of 99.5% purity was purchased from Alfa Aesar and used without further purification. High pressure was generated using a diamond anvil cell (DAC), furnished with 0.4 mm diamond culets. The sample was loaded into a 0.15 mm-diameter aperture in the center of the T301 steel gasket, which had been preindented to a thickness of 70 μm. Two or three ruby balls were also loaded into the sample compartment, so that the ruby fluorescence method could be used to calibrate the pressure.[28] Furthermore, in the two sets of experiments, methanol−ethanol−water (16:3:1, MEW) and silicon oil were used as pressure transmitting medium (PTM) for tuning pressure conditions, respectively. The silicon oil was purchased from Sigma-Adrich (viscosity 10 cst, 25 °C). In the pressure range below 10 GPa, MEW provides a better pressure condition than silicon oil.[29] All of the experiments were performed at room temperature.

In situ angle dispersive X-ray diffraction (ADXRD) measurements with a wavelength of 0.6199 Å were carried out at the 4W2 High-Pressure Station of Beijing Synchrotron Radiation Facility (BSRF). Meanwhile, portions of this work were performed on the BL15U1 beamline (λ = 0.6199 Å) at the Shanghai Synchrotron Radiation Facility (SSRF). Furthermore, the supplementary experiment for getting the accurate diffraction pattern of EuF_3 at 8.4 GPa (λ = 0.4099 Å) was detected at the High Pressure Collaborative Access Team's (HPCAT's) 16 μ_BD beamline facility of the Advanced Photon Source (APS) at Argonne National Laboratory (ANL). The image-plate area detector (Mar345) was adopted to collect diffraction data, and before each experiment, a CeO_2 standard was used to calibrate the geometric parameters. The two-dimensional XRD images were converted into intensity versus 2θ patterns using FIT2D software.[30] Analysis of ADXRD data was performed using the commercial program Materials Studio 5.5 and GSAS software with the graphical EXPGUI user interface.[31] The detailed Rietveld refinement of diffraction patterns provides the evolution of cell volume and parameters. Moreover, the phase content of each phase was obtained by releasing the phase fractions during the refinement. The specific value of phase fractions represents the phase content ratio of the corresponding phases.

In-situ high-pressure PL experiments of EuF_3 were measured with a Quanta Master 40 spectrometer (produced by Photon Technology, Inc.) in reflection mode. The excitation source is the 405 nm line of a violet diode laser with the power of 30 mW. A photomultiplier-equipped monochromator was applied to record the PL spectra. Typical resolution of the spectra in the present study was 0.25 nm.

RESULTS AND DISCUSSION

As depicted in the plot of 0.7 GPa in Figure 2, the commercial EuF_3 is a mixed phases material of α and β phases. The simulation

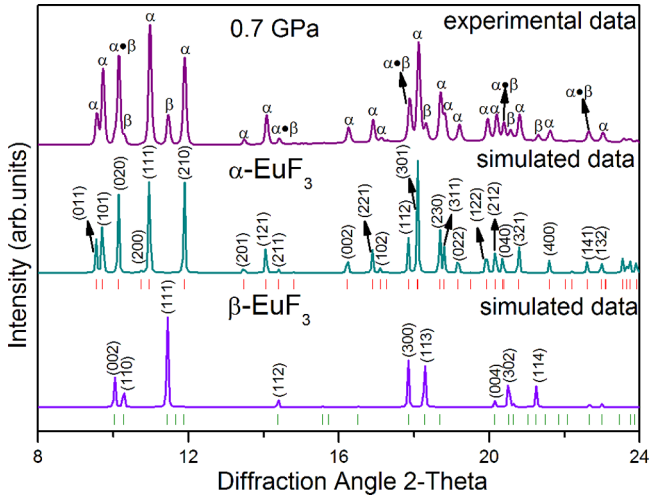

Figure 2. Comparison between the experimental and simulated ADXRD patterns. (top) The diffraction pattern of EuF_3 at 0.7 GPa (peaks of α and β phase are marked, α·β implies the peaks belong to α and β phase simultaneously); (bottom) the simulated diffraction pattern of α-EuF_3 and β-EuF_3 at ambient conditions.

of β-EuF_3 is based on the structural information we solved in this study, which is discussed in a later section. Representative ADXRD patterns of EuF_3 at various pressures are shown in Figure 3. The highest pressure of two sets of experiments is ~10 GPa by the reason that both MEW and silicon oil can keep a relatively good pressure condition in this pressure range. This is a benefit for further refinement of the structure. However, the

dx.doi.org/10.1021/jp412366y | J. Phys. Chem. C 2014, 118, 7562−7568

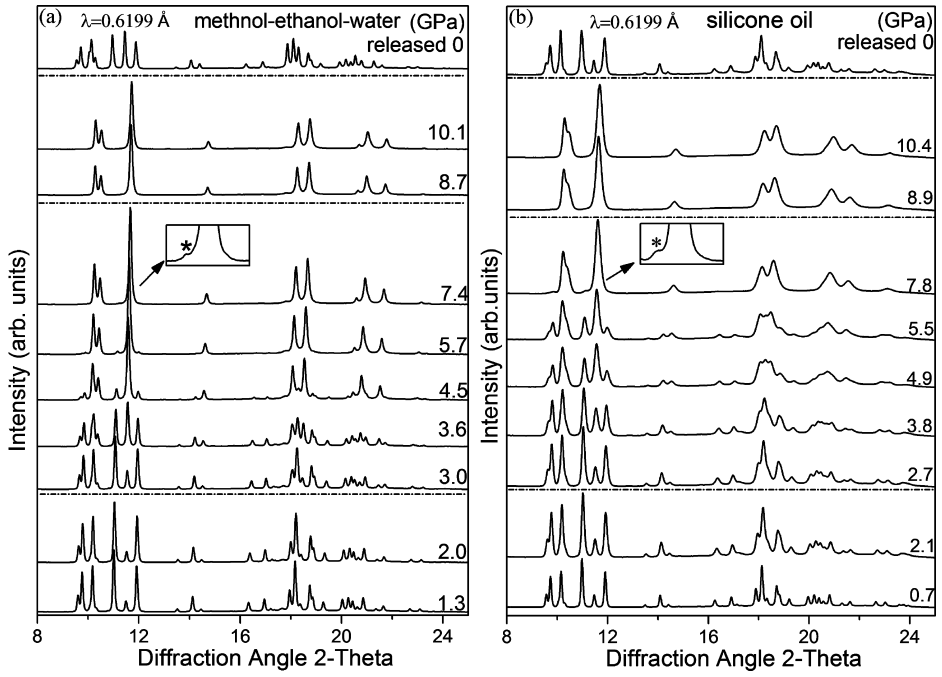

Figure 3. Representative ADXRD diffraction patterns at selected pressures of EuF_3 with the presence of (a) methanol−ethanol−water; (b) silicon oil as PTM during the experiments.

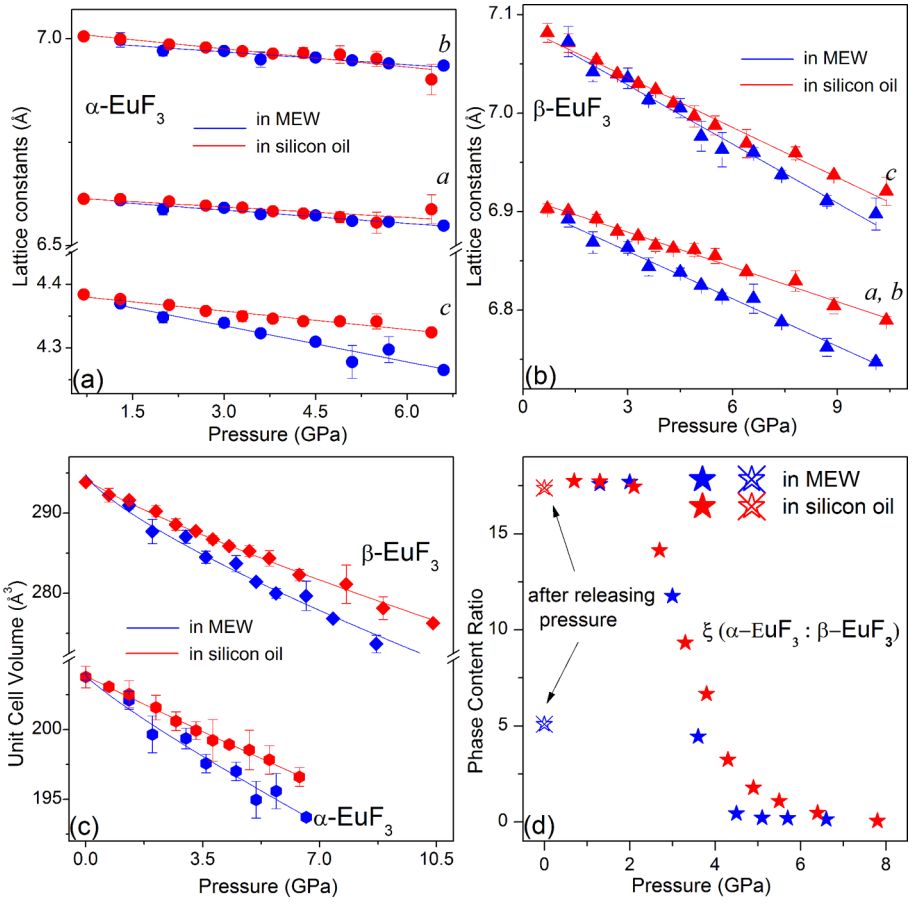

Figure 4. Evolution of the lattice constants of (a) α-EuF_3 and (b) β-EuF_3 with respect to pressure. (c) Pressure dependence of the unit cell volume of β-EuF_3. (d) The phase content ratio (ξ) of α-EuF_3 to β-EuF_3 versus pressure. The data shown in blue and red represent the results in MEW and silicon oil, respectively.

dx.doi.org/10.1021/jp412366y | J. Phys. Chem. C 2014, 118, 7562−7568

pressure condition in the silicon oil is not as good as in MEW. This leads to the fact that broadening of the diffraction peaks in silicon oil is more obvious than that in MEW.[32]

When MEW is adopted as PTM (Figure 3a), below 2.0 GPa, no obvious change is observed, but all of the diffraction peaks shift to higher angles, which results from the expected decrease in lattice parameters, as shown in Figure 4. In the pressure range 3.0−7.4 GPa, the diffraction peaks of α-EuF_3 disappear gradually. And the intensities of peaks belonging to β-EuF_3 get stronger and stronger with increasing pressure, indicating the gradual transition from α-EuF_3 into β-EuF_3. After 8.7 GPa, only the signal of pure β-EuF_3 is obtained, indicative of the accomplishment of the phase transition. In silicon oil (Figure 3b), the results are similar to that in MEW. The pattern of mixed phases EuF_3 remains stable with compression until 2.1 GPa. And the phase transition from α-EuF_3 to β-EuF_3 also exists between 2.7 and 7.8 GPa. After 8.9 GPa, the phase transition is accomplished, and the diffraction data of pure β-EuF_3 remains unchanged until 10.4 GPa is reached. The phase transition of EuF_3 extends over the pressure range of ~4.4 GPa. Such a transition range suggests that the phase transition requires sufficient free energy to overcome the activation barrier.[33,34] That is, there is a high-energy hindrance between the two phases that prevents the rapid phase transition.

Evolution of the parameters in Figure 4 shows the comparison between these two sets of experiments. In this paper, we use the words "poor" and "good" to describe the quality of pressure condition at high pressure. Therefore, the pressure condition in silicon oil is poorer than that in MEW, and nonhydrostatic compression includes contributions from the hydrostatic pressure component and the deviatoric stress component.[35] It has been proven that different pressure conditions are responsible for the different high-pressure response of the lattice parameters,[36,37] broadening of the transition pressure range[38,39] and reversibility of the sample.[40] In EuF_3, as can be seen in Figure 4a−c, the compression of α and β-EuF_3 in silicon oil is more difficult than that in MEW, and the phase content ratio of ξ in Figure 4d, which is defined as the ratio of α-EuF_3 phase to β-EuF_3 phase content, decreases more slowly in silicon oil. This indicates that though the sluggishness of the phase transition is not sufficient enough to broaden the phase transition range, the pressure condition is enough to affect the phase transition rate. Furthermore, it is more important that upon complete release of pressure, ξ in silicon oil is much close to the original value before compression. However, ξ in MEW is much smaller than the original value, implying there is an increasing phase content of β-EuF_3 after the high-pressure treatment in MEW hydrostatic conditions. Such results show that high-pressure treatment is an efficient method to tune the phase content ratio of mixed phases materials. However, the tuning is more effective under better pressure conditions. In a word, comparison between two sets of experiments show that a poor pressure condition is capable of lowering the quality of diffraction data, preventing the compression of EuF_3, making the phase transition more sluggish, and controlling phase content ratio after releasing pressure.

To do structural solving of β-EuF_3, it is better to get an ADXRD pattern with higher intensity and quality. Actually, we have conducted another set of supplementary experiments with MEW at HPCAT in APS to get the diffraction pattern at 8.2 GPa with longer exposure time. Meanwhile, in these further experiments, it has been proven that the structure of β-EuF_3 can remain stable until ~21 GPa is reached. A Rietveld refinement of a pure β-EuF_3 phase at 8.2 GPa is shown in Figure 5. High-pressure β-EuF_3 is best described with trigonal $P\bar{3}c1$, and the indexed lattice parameters are a = 6.785(6) Å, c = 6.934(6) Å

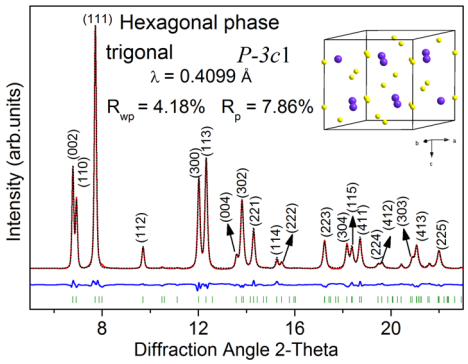

Figure 5. Rietveld refinement of the ADXRD pattern collected at 8.2 GPa. The blue line denotes the difference between the observed (black) and the simulated (red) profiles.

with Z = 6. Commendably, the high-quality ADXRD pattern allows us solving the detailed atomic positions of β-EuF_3 (shown in Table 1). To make the transition path clear, we compare the

Table 1. Atomic Positions for β-EuF_3 at 8.2 GPa

atom	x	y	z
Eu	0.671(3)	0.00	0.25
F(1)	0.332(9)	0.043(2)	0.079(1)
F(2)	0.333(3)	0.666(7)	0.210(5)
F(3)	0.00	0.00	0.25

ambient structure of α-EuF_3 with the structure of β-EuF_3 we solved from the ADXRD pattern at 8.2 GPa (see Figure 6). Through the phase transition, the organization of the structure becomes more regular, and β-EuF_3 is much more compact than α-EuF_3. Structures of both α and β phases are constituted by the overlapped layers of europium atoms, which is coordinated by the surrounding fluorine ions. Through the phase transition, the coordination number of europium anions evolves from 9 to 11, (Figure 6a) exhibiting the compact nature of β-EuF_3, and the positions of the coordination polyhedrons are also adjusted by the external force to form the ordered hexagonal phase structure.

According to the structural models and results of ADXRD experiments, the mechanism of the phase transition of EuF_3 is inferred as follows. At ambient conditions, the coordination number of europium is nine, and the coordination polyhedrons lie in layers along the *ac* plane. At high pressure, the electrostatic interaction is enhanced, as a result of the contraction of interatomic distances. When the α-EuF_3 structure cannot support the increasing free energy anymore, the phase transition to β-EuF_3 occurs to reduce the free energy in the pressure range 2.7−7.8 GPa.[33,34] Through the phase transition, the coordination number of europium ions has increased from 9 to 11, leading to the reconstruction of the coordinated polyhedrons in β-EuF_3.[41] Meanwhile, europium ions form a more ordered arrangement in layers (see Figure 6b,c). Correspondingly, the neighboring polyhedrons in β-EuF_3 become face-shared, accounting for the compact structure. In addition, such transition requires significant free energy to overcome the activation barrier, so the transition extends over a ~4.4 GPa pressure range.[33,34] In general, the β-EuF_3 with highly organized structure is more thermodynamically stable than α-EuF_3.[42] This point is also

dx.doi.org/10.1021/jp412366y | J. Phys. Chem. C 2014, 118, 7562−7568

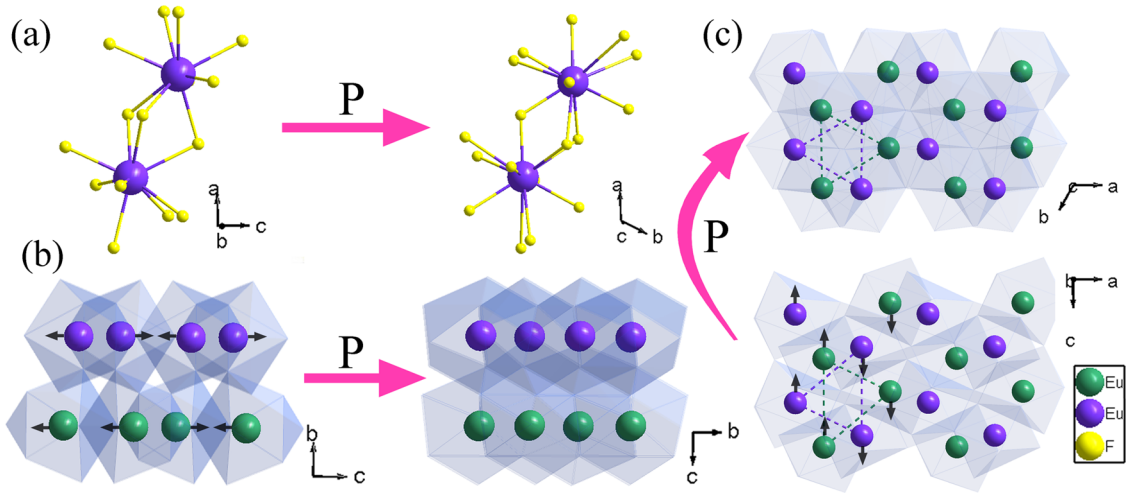

Figure 6. Comparison between the structures of ambient α-EuF_3 and high-pressure β-EuF_3. The black arrows show the moving trends of the europium atom during the phase transition. Europium shown in purple and blues exhibits the atoms in different atom layers.

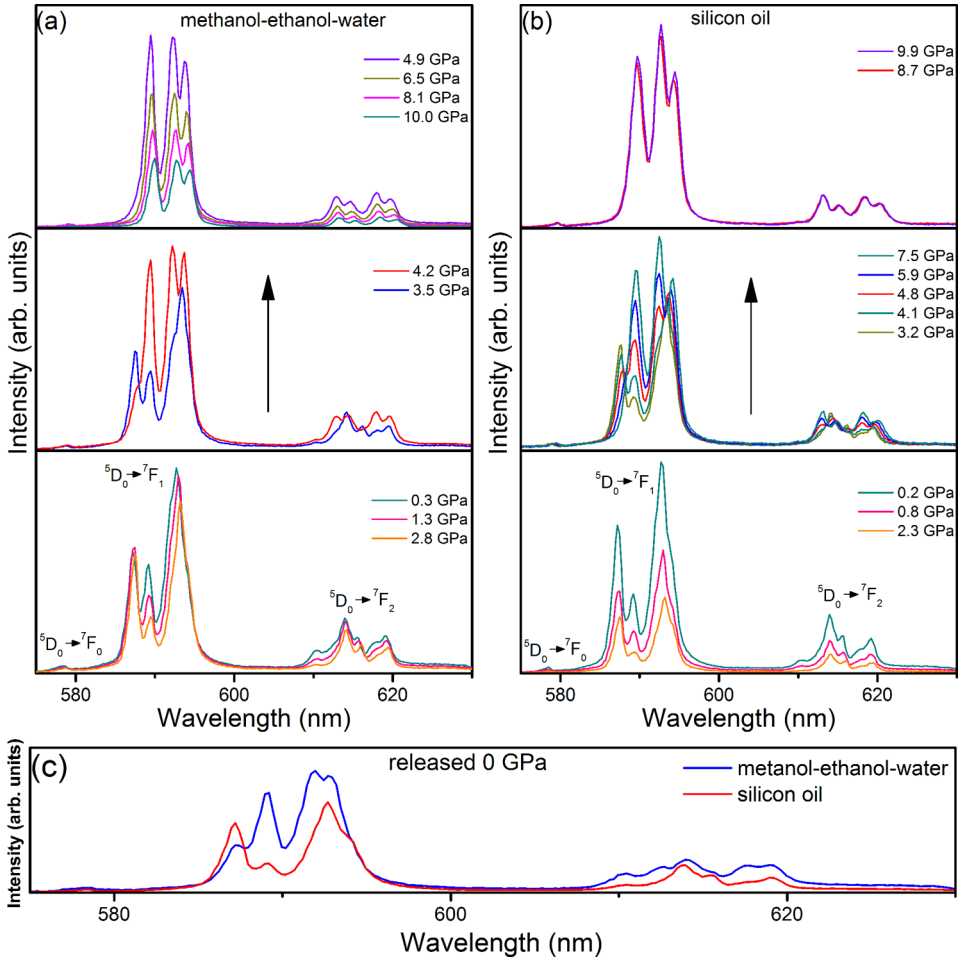

Figure 7. Selected PL spectra of EuF_3 as a function of pressure with the presence of (a) MEW and (b) silicon oil as PTM, respectively. (c) The released patterns in the two cases.

confirmed as the structure of β-EuF_3 keeps stable until ~10 GPa in our experiments.

To explore how the structural transition influences the luminescent properties of mixed phases EuF_3, PL measurements are performed at high pressure. Figure 7 presents the selected PL spectra of EuF_3 for the $^5D_0 \rightarrow ^7F_{0,1,2}$ transition. Initially, the spectrum is the combination of luminescence signals of both α and β phases. All of the emission peaks show the redshift as a function of pressure. When MEW is adopted, as illustrated in Figure 7a, the peaks belonging to β-EuF_3 start to be enhanced at 3.5 GPa, coincident with the proposed phase transition in the pressure range of 3.0−7.4 GPa. Meanwhile, profile of the

dx.doi.org/10.1021/jp412366y | J. Phys. Chem. C 2014, 118, 7562−7568

emission pattern at 4.2 GPa has changed obviously along with the increased intensity. Such an increase is due to the stronger luminescent intensity of β-EuF_3 than that of α-EuF_3.[42] After 4.9 GPa, though the phase transition still continues, only features of β-EuF_3 emission lines are detected for the reason that the stronger emission and increasing phase content of β-EuF_3 lead to the covering of the PL spectra, and preventing the observation of α-EuF_3 spectra. Furthermore, pressure can promote the disordered tendency of EuF_3 and make the sample gasket thinner during compression, leading to the gradually decreased intensities of PL patterns above 4.9 GPa. Overall, at the beginning of the phase transition, the emission intensity of EuF_3 is enhanced.

In silicon oil, the beginning of the phase transition is observed at 3.2 GPa in the PL spectra (Figure 7b). However, similar to ADXRD results, the transition in silicon oil is much more sluggish than that in MEW. Up to 7.5 GPa, the emission peaks of α-EuF_3 have disappeared completely, and the intensities of the patterns remain enhanced, resulting from the persistent slow change of the phase content during the phase transition. The slow transition of the emission spectra in silicon oil supports our conclusion that a poor pressure condition affects the rate of the phase transition, making the transition more sluggish. Furthermore, after releasing pressure, the PL spectra in the two cases are not similar because the recovered ξ are different. We have also performed a repeated compression of EuF_3 to the highest pressure of ~10 GPa with MEW as PTM. There is no obvious change in the released patterns, suggesting that the value of recovered ξ cannot be affected by the repeated compression, and in MEW, when more β-EuF_3 is reserved, the intensity of released PL pattern is stronger than that in silicon oil. Overall, the process of making the mixed phases EuF_3 pure at high pressure is conducive to enhancing the luminescence of the material, and a poor pressure condition is beneficial for keeping the PL intensity of recovered EuF_3, although such enhancement can also be obtained by chemical means of doping lanthanide anions into EuF_3 nanocrystals.[42,43] However, high-pressure treatment is a cleaner method, which meets the need of green chemistry.

CONCLUSION

To sum up, we have experimentally confirmed the pressure-induced phase transition in mixed phases EuF_3, using ADXRD and PL measurements. The EuF_3 of orthorhombic phase α-EuF_3 transfers into its hexagonal phase β-EuF_3 between 2.7 and 7.8 GPa. The detailed structural information of β-EuF_3 is solved for the first time. The mechanism of the transition involves the variations of europium positions in one layer and changes in the coordination number of europium from 9 to 11. Meanwhile, it has proven that a poor pressure condition makes the structure more difficult to compress at high pressure, leading to a more sluggish phase transition, and tuning the phase content ratio of the quenched sample. Furthermore, the PL measurements show that high-pressure treatment of mixed phases EuF_3 is beneficial to the enhancement of its luminescence intensity at extreme conditions. High-pressure explorations on mixed phases EuF_3 can get deeper insight into the relationship of two typical phases of rare-earth trifluorides. This is of crucial importance for extending their application and in designing materials with optimized structures and properties.

AUTHOR INFORMATION

Corresponding Authors

*E-mail: zoubo@jlu.edu.cn. Tel: 86 431 85168882.

*E-mail: kaiwang@jlu.edu.cn.

Notes

The authors declare no competing financial interest.

ACKNOWLEDGMENTS

This work is supported by the National Science Foundation of China (NSFC) (No.91227202), RFDP (No. 20120061130006), and the National Basic Research Program of China (No. 2011CB808200). ADXRD measurements were performed at 4W2 HP-Station, Beijing Synchrotron Radiation Facility (BSRF), which is supported by Chinese Academy of Sciences (Grant KJCX2-SW-N20, KJCX2-SW-N03) and 15U1, Shanghai Synchrotron Radiation Facility (SSRF). Portions of work were performed at HPCAT's beamline facility of the Advanced Photon Source at Argonne National Laboratory. HPCAT is supported by CIW, CDAC, UNLV, and LLNL through funding from DOE-NNSA, DOE-BES, and NSF. APS is supported by DOE-BES (No. DEAC02-06CH11357).

REFERENCES

(1) Ye, X.; Chen, J.; Engel, M.; Millan, J. A.; Li, W.; Qi, L.; Xing, G.; Collins, J. E.; Kagan, C. R.; Li, J.; et al. Competition of Shape and Interaction Patchiness for Self-Assembling Nanoplates. *Nat. Chem.* **2013**, *5*, 466−473.

(2) Lezhnina, M. M.; Jüstel, T.; Kätker, H.; Wiechert, D. U.; Kynast, U. H. Efficient Luminescence from Rare-Earth Fluoride Nanoparticles with Optically Functional Shells. *Adv. Funct. Mater.* **2006**, *16*, 935−942.

(3) Li, C.; Ma, P.; Yang, P.; Xu, Z.; Li, G.; Yang, D.; Peng, C.; Lin, J. Fine Structural and Morphological Control of Rare Earth Fluorides REF_3 (RE = La-Lu, Y) Nano/Microcrystals: Microwave-Assisted Ionic Liquid Synthesis, Magnetic and Luminescent Properties. *Cryst. Eng. Commun.* **2011**, *13*, 1003−1013.

(4) Morrison, C. A.; Leavitt, R. P. Crystal-Field Analysis of Triply Ionized Rare Earth Ions in Lanthanum Trifluoride. *J. Chem. Phys.* **1979**, *71*, 2366−2374.

(5) Lage, M. M.; Righi, A.; Matinaga, F. M.; Gesland, J. Y.; Moreira, R. L. Raman-Spectroscopic Study of Lanthanide Trifluorides with The β-YF_3 Structure. *J. Phys.: Condens. Matter* **2004**, *16*, 3207−3218.

(6) Stouwdam, J. W.; van Veggel, F. C. J. M. Near-Infrared Emission of Redispersible Er^{3+}, Nd^{3+}, and Ho^{3+} Doped LaF_3 Nanoparticles. *Nano Lett.* **2002**, *2*, 733−737.

(7) Wang, L.; Li, P.; Li, Y. Down- and Up-Conversion Luminescent Nanorods. *Adv. Mater.* **2007**, *19*, 3304−3307.

(8) Wang, Z. L.; Quan, Z. W.; Jia, P. Y.; Lin, C. K.; Luo, Y.; Chen, Y.; Fang, J.; Zhou, W.; O'Connor, C. J.; Lin, J. A Facile Synthesis and Photoluminescent Properties of Redispersible CeF_3, CeF_3:Tb^{3+}, and CeF_3:Tb^{3+}/LaF_3 (Core/Shell) Nanoparticles. *Chem. Mater.* **2006**, *18*, 2030−2037.

(9) Chen, D.; Yu, Y.; Huang, F.; Wang, Y. Phase Transition from Hexagonal LnF_3 (Ln = La, Ce, Pr) to Cubic $Ln_{0.8}M_{0.2}F_{2.8}$ (M = Ca, Sr, Ba) Nanocrystals with Enhanced Upconversion Induced by Alkaline-Earth Doping. *Chem. Commun.* **2011**, *47*, 2601−2603.

(10) Yao, M.; Joly, A. G.; Chen, W. Formation and Luminescence Phenomena of LaF_3:Ce^{3+} Nanoparticles and Lanthanide-Organic Compounds in Dimethyl Sulfoxide. *J. Phys. Chem. C* **2009**, *114*, 826−831.

(11) Zalkin, A.; Templeton, D. H. The Crystal Structures of YF_3 and Related Compounds. *J. Am. Chem. Soc.* **1953**, *75*, 2453−2458.

(12) Thoma, R. E.; Brunton, G. D. Equilibrium Dimorphism of the Lanthanide Trifluorides. *Inorg. Chem.* **1966**, *5*, 1937−1939.

(13) Chen, Z.; Geng, Z.; Shi, M.; Liu, Z.; Wang, Z. Construction of EuF_3 Hollow Sub-Microspheres and Single-Crystal Hexagonal Micro-discs via Ostwald Ripening and Oriented Attachment. *Cryst. Eng. Comm.* **2009**, *11*, 1591−1596.

(14) Wang, M.; Huang, Q. L.; Hong, J. M.; Chen, X. T.; Xue, Z. L. Controlled Synthesis and Characterization of Nanostructured EuF_3 with

Different Crystalline Phases and Morphologies. *Cryst. Growth Des.* **2006**, *6*, 2169−2173.
(15) Zhu, L.; Liu, X.; Meng, J.; Cao, X. Facile Sonochemical Synthesis of Single-Crystalline Europium Fluorine with Novel Nanostructure. *Cryst. Growth Des.* **2007**, *7*, 2505−2511.
(16) Wang, M.; Huang, Q. L.; Hong, J. M.; Chen, X. T.; Xue, Z. L. Selective Synthesis and Characterization of Nanocrystalline EuF_3 with Orthorhombic and Hexagonal Structures. *Cryst. Growth Des.* **2006**, *6*, 1972−1974.
(17) Chen, Z.; Geng, Z.; Shao, D.; Mei, Y.; Wang, Z. Single-Crystalline EuF_3 Hollow Hexagonal Microdisks: Synthesis and Application as a Background-Free Matrix for MALDI-TOF-MS Analysis of Small Molecules and Polyethylene Glycols. *Anal. Chem.* **2009**, *81*, 7625−7631.
(18) Li, S.; Li, Q.; Wang, K.; Zhou, M.; Huang, X.; Liu, J.; Yang, K.; Liu, B.; Cui, T.; Zou, G.; Zou, B. Pressure-Induced Irreversible Phase Transition in the Energetic Material Urea Nitrate: A Combined Raman Scattering and X-ray Diffraction Study. *J. Phys. Chem. C* **2013**, *117*, 152−159.
(19) Yuan, H.; Wang, K.; Li, S.; Tan, X.; Li, Q.; Yan, T.; Yang, K.; Liu, J.; Liu, B.; Zou, G.; et al. High-Pressure Stability and Compressibility of Zircon-Type $YV_{1-x}P_xO_4$:Eu^{3+} Solid-Solution Nanoparticles: An X-ray Diffraction and Raman Spectroscopy Study. *J. Phys. Chem. C* **2013**, *117*, 18603−18612.
(20) Lorbeer, C.; Cybińska, J.; Mudring, A. V. Europium (III) Fluoride Nanoparticles from Ionic Liquids: Structural, Morphological, and Luminescent Properties. *Cryst. Growth Des.* **2011**, *11*, 1040−1048.
(21) Zeng, Q. G.; Ding, Z. J.; Zhang, Z. M.; Sheng, Y. Q. Photoluminescence and Raman Spectroscopy Studies of $Eu(OH)_3$ Rods at High Pressures. *J. Phys. Chem. C* **2010**, *114*, 4895−4900.
(22) Crichton, W. A.; Bouvier, P.; Winkler, B.; Grzechnik, A. The Structural Behaviour of LaF_3 at High Pressures. *Dalton Trans.* **2010**, *39*, 4302−4311.
(23) Yuan, H.; Wang, K.; Li, S.; Tan, X.; Li, Q.; Yan, T.; Cheng, B.; Yang, K.; Liu, B.; Zou, G.; Zou, B. Direct Zircon-to-Scheelite Structural Transformation in YPO_4 and YPO_4:Eu^{3+} Nanoparticles Under High Pressure. *J. Phys. Chem. C* **2012**, *116*, 24837−24844.
(24) Spedding, F. H.; Beaudry, B. J.; Henderson, D. C.; Moorman, J. High Temperature Enthalpies and Related Thermodynamic Functions of the Trifluorides of Sc, Ce, Sm, Eu, Gd, Tb, Dy, Er, Tm, and Yb. *J. Chem. Phys.* **1974**, *60*, 1578−1588.
(25) Ranieri, I. M.; Baldochia, S. L.; Klimm, D. The Phase Diagram GdF_3-LuF_3. *J. Solid State Chem.* **2008**, *181*, 1070−1074.
(26) Diniz, E. M.; Paschoal, C. W. A. Structural Phase Transitions under Pressure in Rare Earth Triuorides Compounds with Tysonite Structure. *Solid State Commun.* **2005**, *136*, 538−542.
(27) Zinchenko, V. F.; Efryushina, N. P.; Eryomin, O. G.; Markiv, V. Y.; Belyavina, N. M.; Mozkova, O. V.; Zakharenko, M. I. Synthesis, Structure and Optical Properties of EuF_3 Film-Forming Material. *J. Alloy. Compd.* **2002**, *347*, L1−L3.
(28) Mao, H. K.; Bell, P. M.; Shaner, J. W.; Steinberg, D. J. Specific Volume Measurements of Cu, Mo, Pd, and Ag and Calibration of the Ruby R_1 Fluorescence Pressure Gauge From 0.06 to 1 Mbar. *J. Appl. Phys.* **1978**, *49*, 3276−3283.
(29) Klotz, S.; Chervin, J. C; Munsch, P.; Le Marchand, G. L. Hydrostatic Limits of 11 Pressure Transmitting Media. *J. Phys. D: Appl. Phys.* **2009**, *42*, 075413.
(30) Hammersley, A. P.; Svensson, S. O.; Hanfland, M.; Fitch, A. N.; Häusermann, D. Two-Dimensional Detector Software: From Real Detector to Idealised Image or Two-Theta Scan. *High Pressure Res.* **1996**, *14*, 235−248.
(31) Larson, A. C.; Von Dreele, R. B. *General Structure Analysis System (GSAS)*; Report Number 86748; Los Alamos National Laboratory: Los Alamos, NM, 2004.
(32) Eto, T.; Endo, S.; Imai, M.; Katayama, Y.; Kikegawa, T. Crystal Structure of NiO Under High Pressure. *Phys. Rev. B* **2000**, *61*, 14984−14988.
(33) Yu, X.; Li, M.; Xie, M.; Chen, L.; Li, Y.; Wang, Q. Dopant-Controlled Synthesis of Water-Soluble Hexagonal $NaYF_4$ Nanorods with Efficient Upconversion Fluorescence for Multicolor Bioimaging. *Nano Res.* **2010**, *3*, 51−60.
(34) Dong, C.; Raudsepp, M.; van Veggel, F. C. J. M. Kinetically Determined Crystal Structures of Undoped and La^{3+}-Doped LnF_3. *J. Phys. Chem. C* **2009**, *113*, 472−478.
(35) Singh, A. K.; Balasingh, C. The Lattice Strains in a Specimen (Hexagonal System) Compressed Nonhydrostatically in an Opposed Anvil High Pressure Setup. *J. Appl. Phys.* **1994**, *75*, 4956−4962.
(36) Zhao, J.; Angel, R. J.; Ross, N. L. Effects of Deviatoric Stresses in the Diamond-Anvil Pressure Cell on Single-Crystal Samples. *J. Appl. Crystallogr.* **2010**, *43*, 743−751.
(37) Singh, A. K. X-ray Diffraction from Solids under Nonhydrostatic Compression—Some Recent Studies. *J. Phys. Chem. Solids* **2004**, *65*, 1589−1596.
(38) Shen, L. H.; Li, X. F.; Ma, Y. M.; Yang, K. F.; Lei, W. W.; Cui, Q. L.; Zou, G. T. Pressure-Induced Structural Transition in AlN Nanowires. *Appl. Phys. Lett.* **2006**, *89*, 141903.
(39) Colonna, N.; Profeta, G.; Continenza, A. Effects of Non-hydrostatic Pressure on the Structural and Magnetic Properties of $BaFe_2As_2$. *Phys. Rev. B* **2011**, *83*, 224526.
(40) Grzechnik, A.; Bouvier, P.; Crichton, W. A.; Farina, L.; Köhler, J. Metastable $NaYF_4$ Fluorite at High Pressures and High Temperatures. *Solid State Sci.* **2002**, *4*, 895−899.
(41) Rotereau, K.; Daniel, P.; Desert, A.; Gesland, J. Y. The High-Temperature Phase Transition in Samarium Fluoride, SmF_3: Structural and Vibrational Investigation. *J. Phys.: Condens. Matter* **1998**, *10*, 1431−1446.
(42) Tian, Y.; Hua, R.; Chen, B.; Yu, N.; Zhang, W.; Na, L. Lanthanide Dopant-Induced Phase Transition and Luminescent Enhancement of EuF_3 Nanocrystals. *Cryst. Eng. Comm.* **2012**, *14*, 8110−8116.
(43) Zhao, Q.; Shao, B.; Lv, W.; Jia, Y.; Lv, W.; Jiao, M.; You, H. Doping Alkaline-Earth: A Strategy of Stabilizing Hexagonal GdF_3 at Room Temperature. *Dalton Trans.* **2013**, *42*, 15482−15488.